

Aggregation-Induced Delayed Fluorescence through Seed-Induced Crystallization

Kwang-Won Park and Trisha L. Andrew*



Cite This: *J. Phys. Chem. C* 2022, 126, 17663–17669



Read Online

ACCESS |



Metrics & More

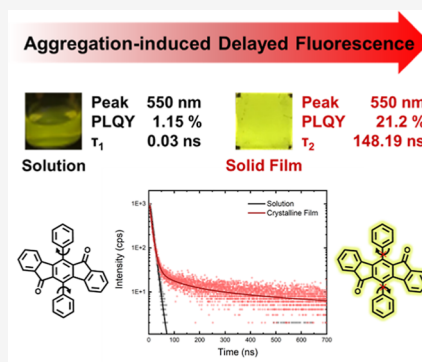


Article Recommendations



Supporting Information

ABSTRACT: Triplet excitons in molecular semiconductor films are integral for producing high-efficiency organic light-emitting diodes. Molecules exhibiting thermally activated delayed fluorescence (TADF) allow for reliable access to triplet excitons without the need for expensive heavy-metal moieties. However, most TADF emitters need to be diluted in a host matrix to prevent self-quenching, which complicates device fabrication and, also, places stringent requirements on charge balance within the device stack that can be easily disrupted with aging. Here, we detail the photophysics of a molecule that displays enhanced quantum yields and delayed fluorescence in neat thin films, without the need for dilution. The aromatic ketone, Dp-IFD, can be organized into crystalline, nanostructured films with an ultrathin coronene seed layer. These crystalline films exhibit enhanced light absorption, amplified emission quantum yields, and longer excited state lifetimes compared to dilute solutions. We use steady-state and time-resolved spectroscopy to confirm that crystalline nanostructured films of Dp-IFD display aggregation-induced delayed fluorescence.



INTRODUCTION

Emissive triplet excitons are integral for high-efficiency organic light-emitting diodes (OLEDs) because of the spin recombination statistics that are operational in these devices. Materials exhibiting thermally activated delayed fluorescence (TADF) allow reliable access to triplet excitons without the need for expensive heavy-metal moieties and enable high exciton utilization.^{1–4} These TADF emitters exhibit narrow energy splitting (ΔE_{ST}) between the first singlet excited state (S_1) and the first triplet excited state (T_1), favorable for efficient reverse intersystem crossing (RISC). According to the spin statistical rules of momentum addition, 25% of all electrically generated excitons are singlets and 75% are triplets.⁵ Therefore, harvesting both singlet and triplet excitons through RISC ensures 100% internal quantum efficiency for high performance OLEDs. Despite these advantages, most conventional TADF materials suffer from self-quenching, that is, aggregation-caused emission quenching (ACQ), and other unproductive exciton annihilation processes in neat films. Therefore, most TADF emitters need to be diluted in a host matrix to prevent self-quenching,^{3,6} which complicates device fabrication and, also, places stringent requirements on charge balance within the device stack that can be easily disrupted with aging.

Recently, several TADF emitters with suppressed ACQ have been developed and employed in non-doped OLEDs. This interesting phenomenon has been termed aggregation-induced emission (AIE), which refers to the luminescence behavior that weakly fluorescent molecules at low concentrations emit strong photoluminescence (PL) upon aggregate formation.^{7–9} AIE materials typically possess constrained molecular structures

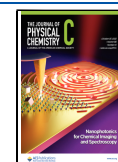
that impede close packing between adjacent molecules, which can effectively inhibit exciton annihilation in the aggregated state. In particular, TADF is compatible with AIE for some molecules, and these emission properties have been termed aggregation-induced delayed fluorescence (AIDF).^{10–14} For example, Tang and co-workers demonstrated a series of AIDF emitters that consist of phenoxazine and benzoyl moieties as electron-donating and -withdrawing units, respectively.¹² These molecules present weak emissions without delayed fluorescence in dilute solutions but strong emissions with delayed fluorescence upon aggregation. These unique properties have made AIDF materials most promising emitting layers for the fabrication of high performance non-doped OLEDs. Thus, non-doped OLEDs based on AIDF emitters have achieved considerable progress in high luminescence efficiency to date.

AIDF materials have often been deposited as amorphous films to utilize AIE in the solid state. Compared to solutions, most of these amorphous films exhibit enhanced emission abilities with “high enough” emission quantum yields for OLED applications. It is common that the highly constrained molecular structures of AIE materials have a strong propensity

Received: June 6, 2022

Revised: September 2, 2022

Published: October 11, 2022



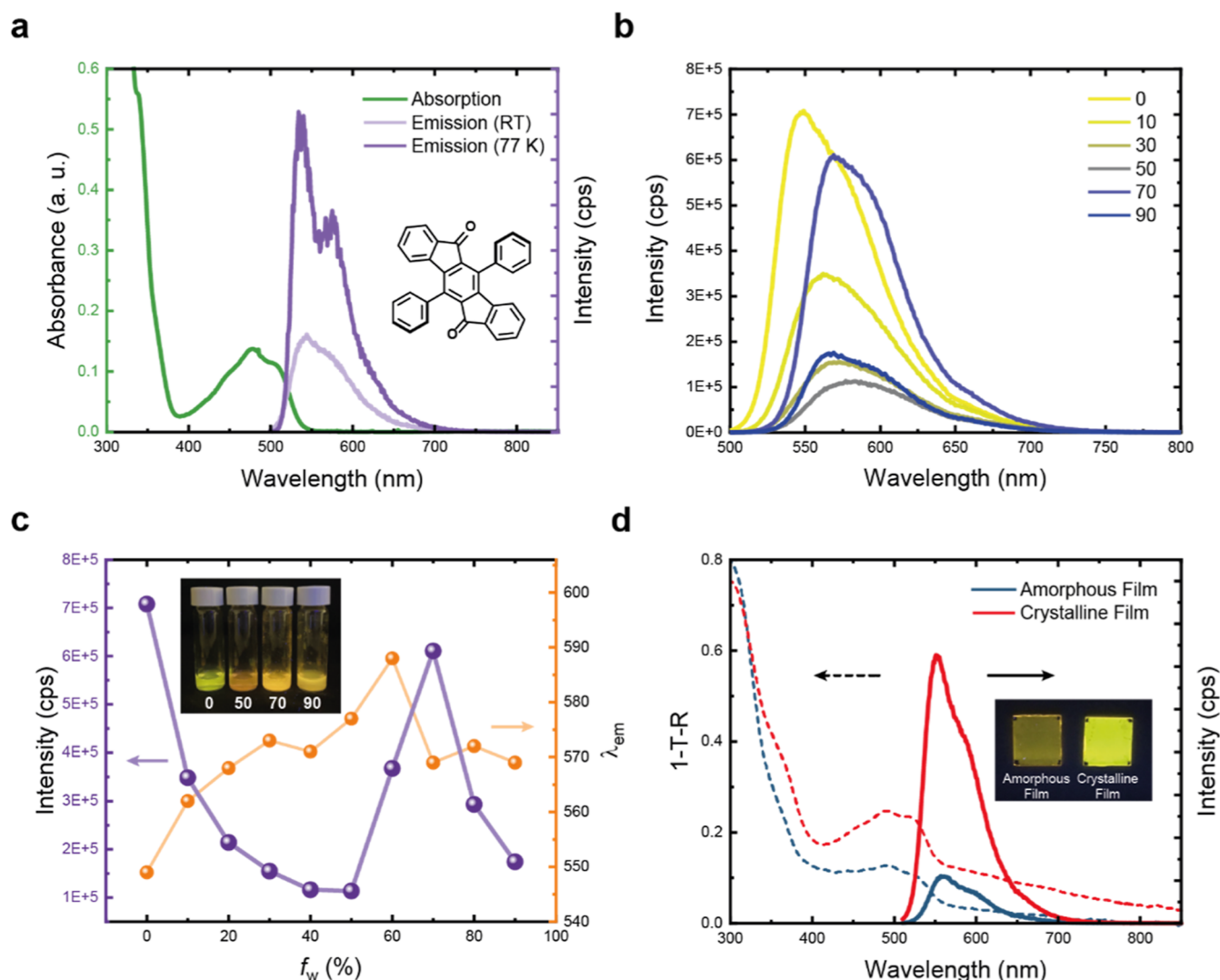


Figure 1. Optical properties of Dp-IFD. (a) UV-vis absorption (left, green) and PL emission spectra (right, purple) of Dp-IFD solution. λ_{ex} for PL spectra is 480 nm. The inset is the chemical structure of Dp-IFD. (b) PL spectra of Dp-IFD in the THF/water mixture with different water fractions (f_w). (c) PL intensity vs f_w of the THF/water mixture. The inset is a photograph of Dp-IFD in THF/water mixtures with 0, 50, 70, and 90% water contents under a UV light. (d) UV-vis absorption (left, dash) and PL spectra (right, solid) of amorphous (blue) and crystalline (red) Dp-IFD films. λ_{ex} for PL spectra is 490 nm. The inset is a photograph of amorphous (left) and crystalline (right) Dp-IFD films on glass substrates under UV light.

for the formation of amorphous films upon fabrication.¹⁵ However, some molecules may have the potential to amplify AIE with “greater” emission quantum yields by further increasing the molecular ordering in the aggregate state. Recently, we have demonstrated a novel coronene seed-induced crystallization method to improve the ordering of molecular films resulting in enhanced optoelectronic characteristics when compared to the amorphous films.¹⁶ Our strategy is conducive to not only better electron transport properties but also higher solid-state PL quantum yields of 5,11-diphenylindeno[1,2-*b*]fluorene-6,12-dione (Dp-IFD, inset of Figure 1a) based on AIE. We also have shown that crystalline nanostructured Dp-IFD films can be applied as an efficient non-doped emitting layer in OLED devices. Here, we investigate the photophysics of Dp-IFD samples in various states to understand the evolution of their delayed fluorescence character upon incorporating our seed-induced crystallization strategy. Dp-IFD exhibits weak emissions without the delayed component in solutions, but emissions become stronger with

delayed fluorescence behaviors once fabricated into films. By comparing the photophysical measurements in different environments, we demonstrate that seed-induced crystalline nanostructured films effectively suppress non-radiative internal conversion channels and promote RISC processes that reinforce AIDF features. Interestingly, our seed-induced method forms unique nanostructured films as a kinetic product that exhibit better emission properties than thermodynamic products obtained by thermal annealing.

EXPERIMENTAL METHODS

All chemical compounds and solvents in this work were received from Sigma-Aldrich and used without further treatment. Si and glass substrates were cleaned subsequently for 10 min each under 0.25% aqueous Micro-90, deionized water, acetone, and 2-propanol in an ultrasonic bath and dried using N_2 gas. The substrates were further treated with UV-ozone for 15 min to remove organic residues on the surface. Organic films were deposited using the commercial thermal

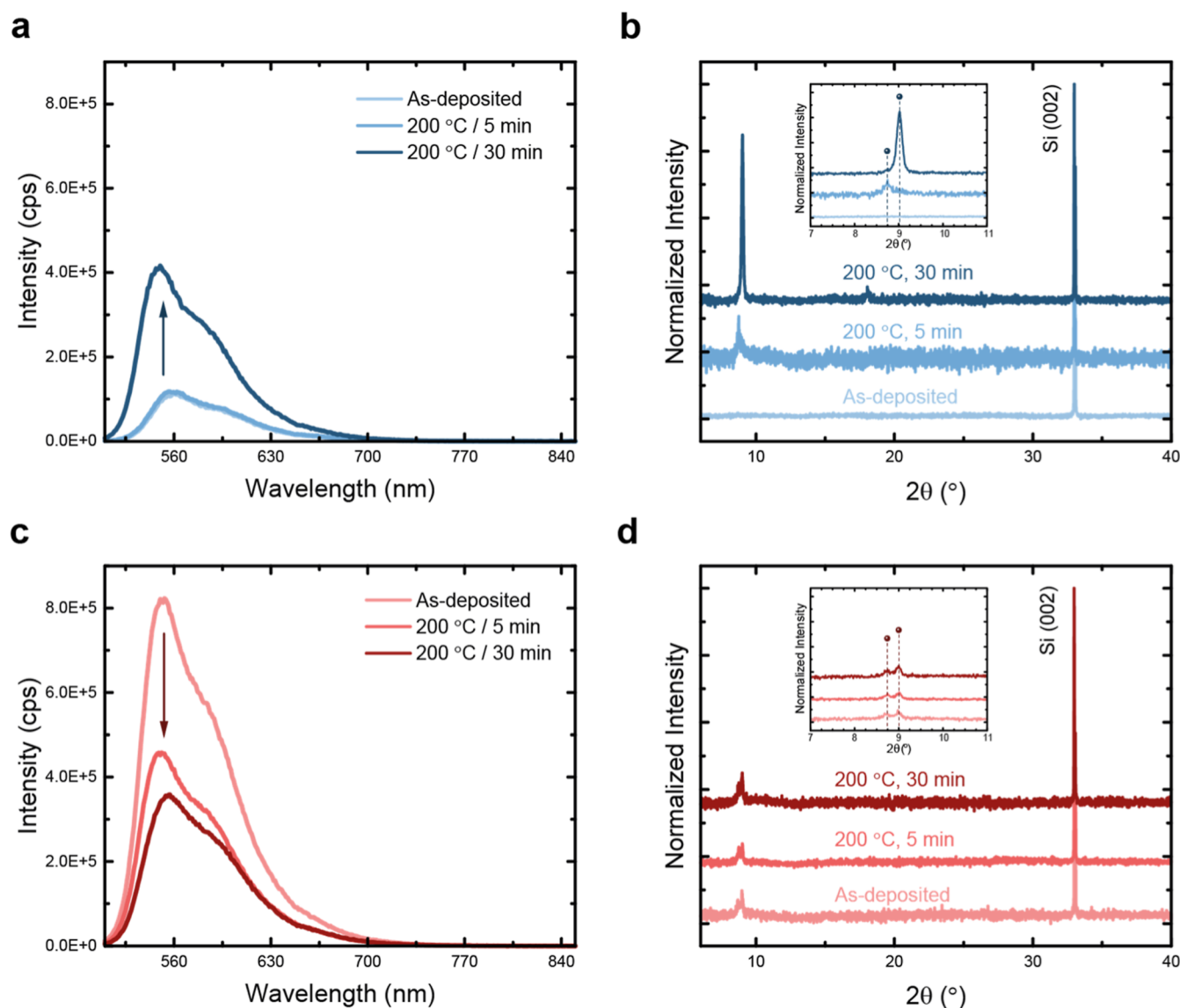


Figure 2. PL spectra and XRD patterns of Dp-IFD films after thermal annealing. (a,c) PL spectra of amorphous (a) and crystalline (c) Dp-IFD thin films, respectively. Films are deposited on glass substrates with the thickness of 100 nm. (b,d) XRD patterns of amorphous (b) and crystalline (d) Dp-IFD thin films, respectively. Insets are the magnified view in the region of the peak of the film.

evaporating system (Angstrom Nexdep) under a base pressure of 5×10^{-7} Torr. During the deposition of Dp-IFD, the source temperature was kept proximately at 220 °C for the growth rate of 0.3 Å/s, which was monitored by a quartz crystal microbalance. UV–vis absorption spectra were obtained using an UV–vis spectrophotometer (Evolution 220, Thermo Scientific), and PL was recorded using a fluorometer (Fluorolog-3, Horiba Scientific). For optical characterizations, all films were prepared on glass substrates. Time-correlated single photon counting accessory with a pulsed monochromatic LED light (NanoLED-370, peak wavelength of 371 nm, Pulse duration of 1.4 ns, Horiba Jobin Yvon Ltd.) was utilized to obtain time-resolved PL characteristics of the samples. After the measurement, the emission decay spectra were analyzed based on first- or second-order kinetics using a Decay Analysis Software manufactured by Horiba Scientific. X-ray diffraction (XRD) patterns of films were measured using SmartLab XRD (Rigaku).

RESULTS AND DISCUSSION

In order to gain deeper insights into the photophysics of isolated Dp-IFD molecules, we first explored the optical properties of Dp-IFD in diluted environments. Figure 1 shows the absorption and emission spectra of 100 μM solution in THF. It can be seen that Dp-IFD has a characteristic π – π^* absorption band at a higher energy region and n – π^* absorption band in the range of 450–500 nm, with a maximum absorption (λ_{\max}) of 478 nm, where the sample is excited to measure the PL spectra. Its THF solution gives a fluorescence quantum yield (ϕ_F) as low as 1.15%. From the PL measurements at RT and 77 K, ΔE_{ST} is estimated as 0.03 eV. Emission bands between fluorescence and phosphorescence look overlapping with each other; however, normalized spectra (Figure S1) clearly show that there is a narrow gap between them. This is widely observed in many other TADF-active materials from previous literature.¹⁷ When water as a non-solvent is added into the solution to induce aggregation, the PL emission intensity and position change (Figure 1b). PL

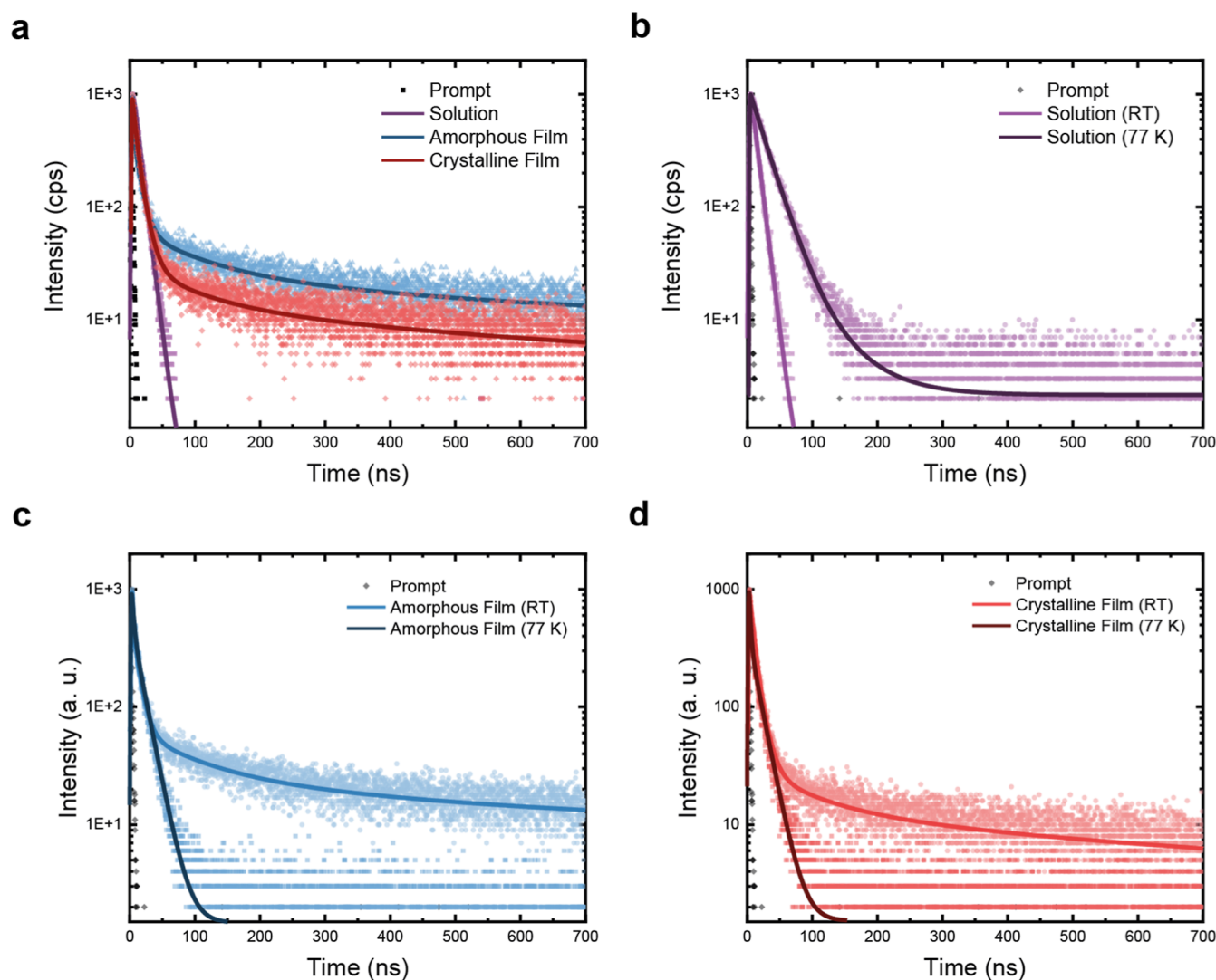


Figure 3. Time-resolved PL spectra of Dp-IFD. (a) PL decay of Dp-IFD solution (purple), amorphous film (blue), and crystalline film (red) as a function of time. (b–d) PL decay of Dp-IFD solution (b), amorphous film (c), and crystalline film (d) obtained at RT (light) and 77 K (dark), respectively.

intensity and emission wavelengths (λ_{em}) are plotted in Figure 1c as a function of the water fraction (f_w) in THF/water mixture solution. After the addition of water, the emission intensity reduced gradually until the f_w reaches 50%, and a red shift of the λ_{max} is also observed from 479 to 486 nm. Meanwhile, the λ_{em} changes more widely as the values vary from 550 to 590 nm, associated with the emission color change under UV light exposure, as shown in the inset of Figure 1c. This might be attributed to the solvatochromic effect, induced by the addition of water as a polar solvent. Afterward, the emission intensity enhances until the f_w reaches 70%. We postulate that bigger aggregates start to form when the $f_w = 50\%$, since UV–vis absorption of these solutions weaken when the $f_w > 50\%$ due to the scattering of the aggregates in solution. These bigger aggregates are even visible by naked eyes as the solutions become opaque with the increasing f_w over 50%. This phenomenon is characterized by AIE of Dp-IFD as the aggregate size increased when the f_w increased.¹⁸ However, further increasing the f_w beyond 70% gave rise to the irregular behaviors of the PL intensity and λ_{em} , possibly due to different aggregation states forming in the presence of water. Figure S2 shows the Stokes shift of the Dp-IFD in the THF/water

mixture with different amounts of the f_w . When the $f_w = 0\%$, the Stokes shift is as low as 70 nm, but as f_w increases, the Stokes shifts broaden to 91 nm until the $f_w = 50\%$, attributable to the bathochromic shift of excited, aggregated states. In contrast, when larger molecular aggregates or crystals are formed ($f_w > 50\%$), the Stokes shift gradually decreases. This is consistent with the AIE of Dp-IFD in its aggregated state: intramolecular motion is more restricted as the aggregates become bigger and rigid with the increasing f_w .

Next, we examined the optical properties of thermally evaporated Dp-IFD thin films for practical purposes. For the preparation of the film samples, we have developed an unprecedented method of incorporating coronene as a nucleation seed layer.¹⁶ In order to create crystalline nanostructures, the ultrathin (<2 nm) layer of coronene was initially applied on the substrate followed by Dp-IFD deposition during the thermal evaporation process. Dp-IFD has a strong intrinsic proclivity to form disordered films in the absence of the seed layer, and thus, the film is regarded as amorphous. However, the coronene seeds effectively induce the crystallization of the subsequent Dp-IFD films, which is regarded as crystalline. The crystallinity of the films was

confirmed by grazing-incident wide angle X-ray scattering (Figure S3) as well as conventional XRD, and the diffraction patterns are matched with previous reported data.¹⁶ In addition, we further confirmed that the negligible amount of the coronene seed layer has no effect on the crystalline Dp-IFD films in terms of optical and electronic interferences between two layers. As shown in Figure 1d, UV–vis absorption and PL spectra of thin film samples resemble those of solution. However, the film samples exhibit a $\lambda_{\text{max}} = 490$ nm, which is red shifted by 12 nm compared to samples in solution (Figure S4), because of aggregates in the film.^{19,20} It is interesting to note that the crystalline film is capable of absorbing slightly more light in the region between 450 and 550 nm than the amorphous film, as shown in the absorption spectrum. This is likely because the crystalline film has nanostructures on the surface where incident light scatters, making the film less reflective. As a result, the crystalline film looks opaque, whereas the amorphous film looks transparent. While the light absorption properties are similar, it is noteworthy that the crystalline film exhibits about 1 order of magnitude higher PL intensity than the amorphous counterpart. The ϕ_{F} is estimated as 21.2% for the crystalline sample, which is 4.3 times higher than that of the amorphous sample ($\phi_{\text{F}} = 4.89\%$). Based on the film morphologies and thin-film X-ray studies in our previous report,¹⁶ we conclude that this phenomenon is explained by crystallization-induced enhanced emission (CIEE) behavior. Furthermore, we observe that the PL emission peak of the amorphous sample is centered at 560 nm, while the peak of the crystalline sample is located at 550 nm. This decreased Stokes shift of the crystalline sample is consistent with the fact that the molecules are more ordered and crystallized in the film and thereby exhibit less reorganization energy in its excited state. We also observed that both thin film samples emit bright yellow light under a UV light excitation, as shown in the inset of Figure 1d.

We further explored the optical properties of the Dp-IFD thin films by post-deposition annealing them at 200 °C as a crystallization temperature. We hypothesized that CIEE can be enhanced by increasing the molecular ordering by thermal treatment. As shown in Figure 2a, thermal annealing of amorphous Dp-IFD films at 200 °C for 5 min does not change the PL intensity. After 30 min, however, the PL intensity increases dramatically nearly four times relative to the as-deposited sample. Figure 2b shows that the crystallinity of the Dp-IFD films gradually increases upon thermal annealing: an ultimately distinctive XRD peak is observed at $2\theta = 9^\circ$ after 30 min. This implies that the thermal annealing process leads to the increased molecular ordering in the films, resulting in enhanced CIEE of the Dp-IFD films. Additionally, the maximum PL peak slightly shifts from 556 to 550 nm, further indicating that molecular ordering increases in the films (Figure 2a).

In contrast, crystalline Dp-IFD films show entirely opposite behaviors compared to the amorphous counterparts. Even 5 min thermal treatment reduces the PL intensity significantly by half, and the PL intensity gradually decreases over 30 min during the thermal annealing at 200 °C (Figure 2c). Including the fact that the maximum PL peak slightly shifts from 550 to 556 nm, the thermal annealing process is detrimental to the PL pathway of the crystalline Dp-IFD thin films. However, XRD patterns of the crystalline Dp-IFD samples do not change significantly upon thermal annealing. Based on these results, we conclude that seed-induced crystalline nanostructures have

kinetically trapped intermolecular conformations with very short-range order, which is unperceived in XRD patterns. Therefore, thermal treatment disrupts the intermolecular conformations in the nanostructures, leading to more possibilities of non-radiative pathways. Although the thermal annealing enhances the PL intensity of the amorphous samples to some extent, the thermodynamic films obtained from the thermal process could not exceed the PL intensity of the kinetically grown crystalline nanostructured films. Rather, higher temperature or longer thermal treatments than 200 °C for 30 min reduce the PL intensity.

Moreover, the photophysical properties were investigated using time-resolved PL measurements of different types of Dp-IFD samples as illustrated in Figure 3, and the resulting photophysical parameters are summarized in Table 1. The PL

Table 1. Photophysical Parameters of Dp-IFD in Different Sample States

status	temperature (K)	ϕ_{F} (%)	τ_1 (ns)	τ_2 (ns)
solution (THF)	293	1.15	9.48	
	77		22.69	57.85
amorphous film	293	4.89	6.62	126.28
	77		2.99	15.4
crystalline film	293	21.20	8.82	148.19
	77		2.14	15.33

of the Dp-IFD solution in THF decays quickly with a short lifetime of 9.48 ns as a result of fluorescence emission. On the other hand, the solid-state samples exhibit notable delayed fluorescence emission with longer lifetimes: $\tau_1 = 6.62$ ns, $\tau_2 = 126.28$ ns for amorphous and $\tau_1 = 8.82$ ns, $\tau_2 = 149.19$ ns for the crystalline film, respectively. Importantly, these delayed components are strongly indicative of the presence of triplet excitons in the light emission process. We first hypothesized that the delayed components of solid-state samples can be caused by triplet–triplet annihilation (TTA) in the aggregate states. To test this hypothesis, we prepared molecular doping samples using 1,4-bis(triphenylsilyl)benzene (UGH) as a wide band gap (4.4 eV) host material. However, 10 wt % doped films still exhibit delayed fluorescence behaviors with $\tau_1 = 3.73$ ns, $\tau_2 = 131.60$ ns, which resemble the amorphous films (Figure S5a). This indicates that the delayed fluorescence of Dp-IFD is not because of intermolecular associations, such as the TTA, but because of intrinsic molecular properties. In addition, we can infer that intermolecular excitonic interactions in Dp-IFD films are negligible because the PL intensity of the 100 nm-thick 10 wt % doped films is equivalent to that of the 10 nm-thick amorphous films (Figure S5b). This also shows that Dp-IFD molecules are well dispersed and remained as amorphous in the UGH matrix without host–guest interactions.

Based on the narrow ΔE_{ST} of 0.03 eV (Figure 1a), another possibility is that the delayed components could be a result of TADF behaviors. To confirm whether the PL decay of Dp-IFD comes from TADF, we performed PL decay experiments at different temperatures. However, the PL decays of solution obtained at RT and 77 K (Figure 3b) cannot be explained by TADF. The solution exhibits longer lifetime at lower temperatures, whereas both amorphous (Figure 3c) and crystalline films (Figure 3d) exhibit the longer lifetime of PL at higher temperatures. This interesting emission behavior is

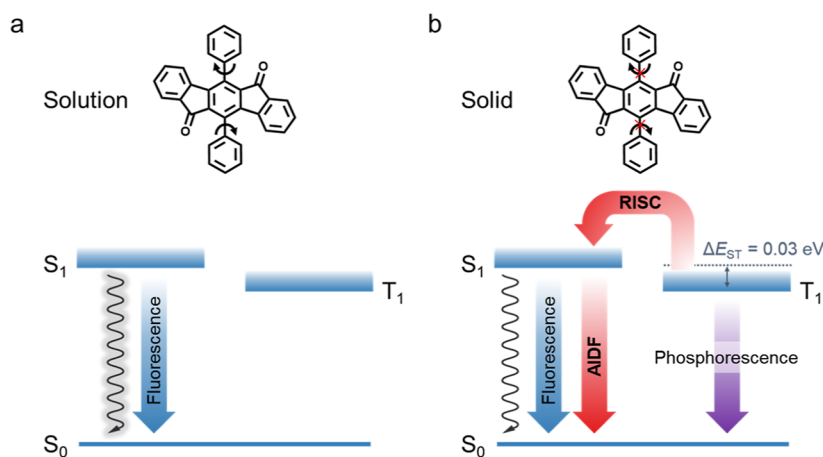


Figure 4. Jablonski diagram of Dp-IFD (a) in solutions and (b) in solids.

attributable to the AIDF effect of the Dp-IFD molecules at different states.

Since the intramolecular rotation of phenyl moieties has a great influence on the PL emissions of the AIE active materials, the restriction of this rotational motion is a prerequisite for delayed fluorescence. The PL of the Dp-IFD solution at RT decays quicker because the phenyl rotation is very active in the diluted environment, while this motion is sufficiently impeded at 77 K. This accounts for the longer decay of the Dp-IFD solution at low temperatures (Figure 3b). In thin film samples, however, the Dp-IFD molecules are already in the condensed phase and the intramolecular rotation is also prohibited. Thus, the film samples show longer PL lifetimes at RT compared to 77 K, owing to the higher RISC probability at higher temperatures as TADF materials. Figure 4 shows the Jablonski diagram of Dp-IFD photophysical processes in different states. Although Dp-IFD has no distinct phosphorescence emissions, RISC is very active even at RT due to the narrow ΔE_{ST} (Figure 4b). This gives rise to AIDF behaviors of Dp-IFD samples in aggregated states, making Dp-IFD more useful in solid-state electroluminescence device applications, such as non-doped OLEDs. Otherwise, the excited state of Dp-IFD decays non-radiatively under dilute conditions, such as in solution, mainly because of the rotational motion (Figure 4a). This results in lower emission quantum yields as well as the lack of delayed components during the decay. Furthermore, in conjunction with the enhanced spin–orbit coupling capability of carbonyl moiety,^{1,21,22} RISC is likely to occur during the decay of the excited state of Dp-IFD.

CONCLUSIONS

In summary, we explored the photophysical properties of Dp-IFD as a molecular semiconductor possessing an indeno-fluorene backbone and phenyl substituents. Due to the carbonyl moieties in the molecule, Dp-IFD exhibited characteristic $n-\pi^*$ transitions with a λ_{\max} of 478 nm, and the corresponding yellow PL emission was observed between 550 and 600 nm. In solution, the PL intensity and λ_{em} behave irregularly by increasing the f_w in the THF/water mixture because of the formation of different aggregation states in the presence of water as a polar non-solvent. We found that thermally evaporated Dp-IFD thin films exhibited much higher PL intensities due to AIE. It is noteworthy that seed-induced crystalline nanostructured films showed 4.3 times higher ϕ_F (21.2%) than amorphous counterparts (4.89%). We examined

the influence of crystallinity on the PL emissions by thermal annealing and concluded that crystalline films with kinetically grown nanostructures are beneficial for higher emissions rather than thermodynamic products from thermal treatments. We explored the time-dependent PL decays of Dp-IFD samples in different states and found that Dp-IFD showed delayed fluorescence behaviors only when the intramolecular motion is restricted in the aggregate state. These interesting photophysical properties were characterized by AIDF behaviors owing to the narrow ΔE_{ST} that facilitates RISC. Given that the crystalline film exhibits brighter emissions with higher quantum yield and longer lifetimes, we conclude that seed-induced crystalline nanostructures are advantageous to improve the photophysical properties of Dp-IFD that entails bulky and rotatable phenyl substituents in its molecular structure. This work provides an important insight into creating crystalline nanostructures for enhancing the photophysical properties of molecular semiconductor thin films. Based on the knowledge gained in this effort, we can potentially create crystalline films of AIE-active materials, which should display interesting photophysical properties for efficient light emitting layers.

ASSOCIATED CONTENT

Supporting Information

The Supporting Information is available free of charge at <https://pubs.acs.org/doi/10.1021/acs.jpcc.2c03921>.

Additional material on the spectroscopic data of Dp-IFD (PDF)

AUTHOR INFORMATION

Corresponding Author

Trisha L. Andrew – Department of Chemistry, University of Massachusetts Amherst, Amherst, Massachusetts 01003, United States; Department of Chemical Engineering, University of Massachusetts Amherst, Amherst, Massachusetts 01003, United States; orcid.org/0000-0002-8193-2912; Email: tandrew@umass.edu

Author

Kwang-Won Park – Department of Chemistry, University of Massachusetts Amherst, Amherst, Massachusetts 01003, United States; orcid.org/0000-0002-2700-7005

Complete contact information is available at:

<https://pubs.acs.org/10.1021/acs.jpcc.2c03921>

Notes

The authors declare no competing financial interest.

ACKNOWLEDGMENTS

Financial support from the National Science Foundation (CBET 1706633) is acknowledged. The X-ray diffractometer used in this work was supported by the National Science Foundation Major Research Instrumentation Program (CHE 1726578). K.P. thanks David Bilger for helpful discussion.

REFERENCES

- (1) Chen, Z.; Ni, F.; Wu, Z.; Hou, Y.; Zhong, C.; Huang, M.; Xie, G.; Ma, D.; Yang, C. Enhancing Spin–Orbit Coupling by Introducing a Lone Pair Electron with p Orbital Character in a Thermally Activated Delayed Fluorescence Emitter: Photophysics and Devices. *J. Phys. Chem. Lett.* **2019**, *10*, 2669–2675.
- (2) Hirata, S.; Sakai, Y.; Masui, K.; Tanaka, H.; Lee, S. Y.; Nomura, H.; Nakamura, N.; Yasumatsu, M.; Nakanotani, H.; Zhang, Q.; Shizu, K.; Miyazaki, H.; Adachi, C. Highly efficient blue electroluminescence based on thermally activated delayed fluorescence. *Nat. Mater.* **2015**, *14*, 330–336.
- (3) Liu, Y.; Li, C.; Ren, Z.; Yan, S.; Bryce, M. R. All-organic thermally activated delayed fluorescence materials for organic light-emitting diodes. *Nat. Rev. Mater.* **2018**, *3*, 18020.
- (4) Zhao, J.; Chen, X.; Yang, Z.; Liu, T.; Yang, Z.; Zhang, Y.; Xu, J.; Chi, Z. Highly-Efficient Doped and Nondoped Organic Light-Emitting Diodes with External Quantum Efficiencies over 20% from a Multifunctional Green Thermally Activated Delayed Fluorescence Emitter. *J. Phys. Chem. C* **2019**, *123*, 1015–1020.
- (5) Mikhnenko, O. V.; Blom, P. W.; Nguyen, T.-Q. Exciton diffusion in organic semiconductors. *Energy Environ. Sci.* **2015**, *8*, 1867–1888.
- (6) Cui, L. S.; Nomura, H.; Geng, Y.; Kim, J. U.; Nakanotani, H.; Adachi, C. Controlling singlet–triplet energy splitting for deep-blue thermally activated delayed fluorescence emitters. *Angew. Chem., Int. Ed.* **2017**, *56*, 1571–1575.
- (7) Guan, J.; Shen, C.; Peng, J.; Zheng, J. What Leads to Aggregation-Induced Emission? *J. Phys. Chem. Lett.* **2021**, *12*, 4218–4226.
- (8) Mei, J.; Leung, N. L.; Kwok, R. T.; Lam, J. W.; Tang, B. Z. Aggregation-induced emission: together we shine, united we soar! *Chem. Rev.* **2015**, *115*, 11718–11940.
- (9) Sych, G.; Simokaitiene, J.; Bezikonny, O.; Tsiko, U.; Volyniuk, D.; Gudeika, D.; Grazulevicius, J. V. Exciplex-Enhanced Singlet Emission Efficiency of Nondoped Organic Light Emitting Diodes Based on Derivatives of Tetrafluorophenylcarbazole and Tri/Tetraphenylethylene Exhibiting Aggregation-Induced Emission Enhancement. *J. Phys. Chem. C* **2018**, *122*, 14827–14837.
- (10) Fu, Y.; Chen, H.; Zhao, Z.; Tang, B. Z. Aggregation-induced delayed fluorescence. *Handbook of Aggregation-Induced Emission*; Wiley Online Books, 2022; pp 221–250.
- (11) Furue, R.; Nishimoto, T.; Park, I. S.; Lee, J.; Yasuda, T. Aggregation-Induced Delayed Fluorescence Based on Donor/Acceptor-Tethered Janus Carborane Triads: Unique Photophysical Properties of Nondoped OLEDs. *Angew. Chem., Int. Ed.* **2016**, *55*, 7171–7175.
- (12) Guo, J.; Fan, J.; Lin, L.; Zeng, J.; Liu, H.; Wang, C. K.; Zhao, Z.; Tang, B. Z. Mechanical Insights into Aggregation-Induced Delayed Fluorescence Materials with Anti-Kasha Behavior. *Adv. Sci.* **2019**, *6*, 1801629.
- (13) Guo, J.; Zhao, Z.; Tang, B. Z. Purely organic materials with aggregation-induced delayed fluorescence for efficient nondoped OLEDs. *Adv. Opt. Mater.* **2018**, *6*, 1800264.
- (14) Wu, K.; Wang, Z.; Zhan, L.; Zhong, C.; Gong, S.; Xie, G.; Yang, C. Realizing Highly Efficient Solution-Processed Homo Junction-Like Sky-Blue OLEDs by Using Thermally Activated Delayed Fluorescent Emitters Featuring an Aggregation-Induced Emission Property. *J. Phys. Chem. Lett.* **2018**, *9*, 1547–1553.
- (15) Qin, W.; Yang, Z.; Jiang, Y.; Lam, J. W.; Liang, G.; Kwok, H. S.; Tang, B. Z. Construction of efficient deep blue aggregation-induced emission luminogen from triphenylethene for nondoped organic light-emitting diodes. *Chem. Mater.* **2015**, *27*, 3892–3901.
- (16) Park, K.-W.; Vijayan, R.; Andrew, T. L. Large-Area Heteroepitaxial Nanostructuring of Molecular Semiconductor Films for Enhanced Optoelectronic Response in Flexible Electronics. *Adv. Funct. Mater.* **2022**, *32*, 2113085.
- (17) Hosokai, T.; Matsuzaki, H.; Nakanotani, H.; Tokumaru, K.; Tsutsui, T.; Furube, A.; Nasu, K.; Nomura, H.; Yahiro, M.; Adachi, C. Evidence and Mechanism of Efficient Thermally Activated Delayed Fluorescence Promoted by Delocalized Excited States. *Sci. Adv.* **2017**, *3*, No. e1603282.
- (18) Chen, M.; Hu, X.; Liu, J.; Li, B.; Leung, N. L.; Viglianti, L.; Cheung, T. S.; Sung, H. H.; Kwok, R. T.; Williams, I. D.; Qin, A.; Lam, J. W. Y.; Tang, B. Z. Rational design of red AIEgens with a new core structure from non-emissive heteroaromatics. *Chem. Sci.* **2018**, *9*, 7829–7834.
- (19) Gierschner, J.; Lüer, L.; Milián-Medina, B.; Oelkrug, D.; Egelhaaf, H.-J. Highly Emissive H-Aggregates or Aggregation-Induced Emission Quenching? The Photophysics of All-Trans para-Distyrylbenzene. *J. Phys. Chem. Lett.* **2013**, *4*, 2686–2697.
- (20) Spano, F. C. The Spectral Signatures of Frenkel Polarons in H- and J-Aggregates. *Acc. Chem. Res.* **2010**, *43*, 429–439.
- (21) Anslyn, E. V.; Dougherty, D. A. *Modern Physical Organic Chemistry*; University Science Books, 2006.
- (22) Yang, Z.; Mao, Z.; Zhang, X.; Ou, D.; Mu, Y.; Zhang, Y.; Zhao, C.; Liu, S.; Chi, Z.; Xu, J.; et al. Intermolecular Electronic Coupling of Organic Units for Efficient Persistent Room-Temperature Phosphorescence. *Angew. Chem., Int. Ed.* **2016**, *55*, 2181–2185.

Recommended by ACS

Thermally Activated Delayed Fluorescence Amorphous Molecular Materials for High-Performance Organic Light-Emitting Diodes

Xu-Lin Chen, Can-Zhong Lu, et al.

SEPTEMBER 22, 2021
ACS APPLIED MATERIALS & INTERFACES

READ 

Thermally Activated Lasing in Organic Microcrystals toward Laser Displays

Tongjin Zhang, Yong Sheng Zhao, et al.

NOVEMBER 19, 2021
JOURNAL OF THE AMERICAN CHEMICAL SOCIETY

READ 

Nanotechnology-Assisted, Single-Chromophore-Based White-Light-Emitting Organic Materials with Bioimaging Properties

Arif Hassan Dar, Govindasamy Jayamurugan, et al.

DECEMBER 29, 2021
LANGMUIR

READ 

A Simple Molecular Design Strategy for Delayed Fluorescence toward 1000 nm

Daniel G. Congrave, Hugo Bronstein, et al.

OCTOBER 29, 2019
JOURNAL OF THE AMERICAN CHEMICAL SOCIETY

READ 

Get More Suggestions >